UNCLASSIFIED

Copy 21

~~CONFIDENTIAL~~

NASA TM X-500

NASA TM X-500

TECHNICAL MEMORANDUM

X-500

FREE-FLIGHT INVESTIGATION OF THE STATIC STABILITY AND AERODYNAMIC DRAG OF THREE BLUNT-NOSED CYLINDER-FLARE TEST BODIES AT MACH NUMBERS FROM 13 TO 17

By Ellis E. Whiting and Robert J. Carros

Ames Research Center
Moffett Field, Calif.

UNCLASSIFIED

CLASSIFICATION CHANGE NO. 5/5-71, EFF. 10/15/71

CLASSIFIED DOCUMENT - TITLE UNCLASSIFIED

This material contains information affecting the national defense of the United States within the meaning of the espionage laws, Title 18, U.S.C., Secs. 793 and 794, the transmission or revelation of which in any manner to an unauthorized person is prohibited by law.

NATIONAL AERONAUTICS AND SPACE ADMINISTRATION

WASHINGTON March 1961

~~CONFIDENTIAL~~

UNCLASSIFIED

15752

UNCLASSIFIED

[redacted]

NATIONAL AERONAUTICS AND SPACE ADMINISTRATION

TECHNICAL MEMORANDUM X-500

FREE-FLIGHT INVESTIGATION OF THE STATIC STABILITY AND AERODYNAMIC DRAG OF THREE BLUNT-NOSED CYLINDER-FLARE TEST BODIES AT MACH NUMBERS FROM 13 TO 17*

By Ellis E. Whiting and Robert J. Carros

SUMMARY

The body shapes tested were axially symmetric blunt-nosed cylinders followed by conical flares similar to a class of bodies presently of interest as the re-entry stage on ballistic missiles. The static stability of these test bodies conformed to the characteristics typical of bodies of this general shape at hypersonic velocities, specifically the low initial static stability and the rapid nonlinear increase in stability with angle of attack.

Comparison is made between the experimentally determined static stability and predictions by the Newtonian impact theory and an estimation procedure reported in NASA TM X-377. The Newtonian impact theory is found to seriously overpredict the stability and in one case indicates considerable static stability where, in fact, instability exists. The newer theory gives a very good prediction of the initial stability but does not give the strong favorable nonlinearity of the pitching moment with angle of attack.

INTRODUCTION

The severe heating and stability effects encountered during ballistic re-entry into the earth's atmosphere impose critical restrictions on the variety of shapes acceptable as possible re-entry vehicles. One class of bodies which has been employed for this purpose is characterized by a blunt-nosed cylinder followed by a conical flare. The

*Title, Unclassified

[redacted]

UNCLASSIFIED

blunt nose is provided to reduce the aerodynamic heating and the flare is provided to increase the aerodynamic stability.

The static stability of this class of bodies has been studied experimentally in wind tunnels (e.g., ref. 1) and in the Ames Supersonic Free-Flight Wind Tunnel (refs. 2 and 3). Reference 3 contains some otherwise unpublished wind-tunnel, ballistic-range, and full-scale test results as well as the Ames data. The results presented in reference 1, for a very blunt member of this class, show nearly a constant value for the static pitching moment between Mach numbers of 1.0 and 2.2. These data do, however, show a slight increase in the stabilizing moment above a Mach number of about 2.0. The wind-tunnel and ballistic-range results presented in reference 3 indicate for one shape that the static stability markedly increases between Mach numbers of 2 and 4 and appears to be approaching the value given by Newtonian impact theory for $M \gg 1$. Instead of reaching the Newtonian value, however, the static moment drops sharply between Mach numbers of about 4 and 10 (e.g., refs. 2 and 3) and seems to approach a minimum limit in the region of Mach number 15 (see ref. 3). References 2 and 3 also report a strong increase in the pitching moment with angle of attack, indicating that the relationship governing the pitching moment must contain terms nonlinear as well as linear in pitching amplitude.

The validity of the Newtonian theory for determining the static stability of such configurations was discussed in reference 3. There it was pointed out that this theory fails to give a reliable prediction because the Newtonian flow model, characterized by a single, closely wrapped shock wave, is not realized. An alternative method of analysis was developed and described. This method is based on the existence of a bow wave similar to that given by blast-wave theory and a separate shock wave generated by the flare.

A series of exploratory tests was made at Mach numbers from 13 to 17 of three configurations. The purpose was to make a rapid survey of the aerodynamic behavior of such bodies in the hypersonic speed range and to provide data for the evaluation of the available theoretical methods of stability prediction. Because of the nonlinear variation of static stability with angle of attack, it was necessary to employ novel methods of data analysis (refs. 4 and 5).

SYMBOLS

A reference area, cross-sectional area at nose-cylinder junction

a maximum amplitude of pitching motion

C_D drag coefficient, $\frac{\text{drag}}{qA}$

C_m pitching-moment coefficient, $\frac{M}{qAl}$

C_{m_σ} rate of change of pitching-moment coefficient with angle of attack, $\frac{dC_m}{d\sigma}$

$C_{m_{\sigma_L}}$ value of C_{m_σ} obtained from free-flight angle history with assumption that C_m is linear with σ

C_N normal-force coefficient, $\frac{\text{normal force}}{qA}$

d diameter of missile at nose-cylinder junction

A 4 5 6

I moment of inertia about an axis through the center of gravity and perpendicular to the axis of symmetry

K constant defined in equation (6)

l total missile length

M aerodynamic restoring moment about the center of gravity; positive when directed so that the angle of attack tends to increase

M_∞ Mach number of undisturbed air relative to missile

q dynamic pressure of undisturbed airstream, $\frac{1}{2}\rho V^2$

R Reynolds number

V velocity of missile relative to free stream

$\frac{X_{cg}}{l}$ center-of-gravity location from nose in percent of length

$\frac{X_{cp}}{l}$ center-of-pressure location from nose in percent of length

α angle of attack (in vertical plane)

β angle of sideslip (in horizontal plane)

λ wave length of pitching motion relative to airstream

μ dynamic viscosity of the undisturbed airstream

ω frequency of pitching motion

ρ density of undisturbed airstream

σ absolute magnitude of resultant angle of attack

σ_{eff} angle of attack at which $C_{m_{\sigma_L}} = C_{m_\sigma}$

$\sqrt{\overline{\sigma^2}}$ root mean square angle of attack

$\ddot{\sigma}$ $\frac{d^2\sigma}{dt^2}$

φ initial phase angle in expression for σ (eq. (3))

MODELS AND TEST EQUIPMENT

Three blunt-nosed models with conical flares (figs. 1(a), (b), (c)) were test-flown in the Supersonic Free-Flight Wind Tunnel at Mach numbers from 13 to 17. The models were of a bimetallic construction, tungsten alloy steel and aluminum, to control the center-of-gravity location. Launching of the test bodies to the high Mach numbers reported was accomplished by shooting the models from a light-gas gun upstream through a Mach number 3 airstream. The maximum velocity reached during the tests was 11,500 feet per second (airstream velocity of 2000 ft/sec plus model velocity of 9500 ft/sec). In comparison to the speed of sound in the free stream of 666 feet per second this velocity corresponded to a Mach number of 17.26.

The gun used to launch the test models utilizes a gas of light molecular weight (in this case, helium) for the propellant. The helium is compressed to high temperature and pressure by burning a charge of high explosive gun powder in the pump tube where the helium is chambered. The compressed and heated helium then drives the model from the gun. A description of the principles of operation of guns of this type can be found in reference 6.

Along the test section of the wind tunnel are nine photographic and timing stations. At each of these stations orthogonal shadowgraphs are taken of the model in flight and the time increments between the stations are recorded. From these data the pitching, swerving, and acceleration history of the flight and the aerodynamic characteristics of the model can be determined. Records of the pitching amplitude from two tests made with model A are shown in figure 2. Figure 3 displays the motion in the α, β plane of the same two tests.

METHOD OF DATA ANALYSIS

Until recently the primary method of reducing the basic data recorded in a free-flight facility for axially symmetric bodies has been to assume the pitching-moment coefficient to be a linear function of angle of attack, and the damping to be zero. In such a case, the equation of motion in polar form for planar motion is

$$I\ddot{\sigma} = M = C_m qAl = C_{m_{\sigma_L}} qAl\sigma \tag{1}$$

or

$$\ddot{\sigma} - \frac{C_{m_{\sigma_L}} qAl}{I}\sigma = 0 \tag{2}$$

If $C_{m_{\sigma_L}}$ is negative (corresponding to stable motions) the solution of (2) is the simple harmonic expression which can be written

$$\sigma = a \sin(\omega t + \varphi) \tag{3}$$

Where ω, the angular frequency, is

$$\omega = \sqrt{\frac{-C_{m_{\sigma_L}} qAl}{I}} = \frac{2\pi V}{\lambda} \tag{4}$$

yielding

$$C_{m_{\sigma_L}} = -\frac{(2\pi)^2}{\lambda^2}\frac{2I}{\rho Al} \tag{5}$$

From equations (3) and (5) it is evident that if the assumption of a linear pitching moment is valid, a plot of resultant angle of attack versus time (or distance) will for planar motion be a sine wave, and, more generally, will be a simple harmonic motion. The wave length λ will be independent of amplitude. Figure 2 shows that for test model A, both of these conditions are violated and it is therefore to be expected that the true expression for the pitching moment will contain terms nonlinear in pitching amplitude. The value of $C_{m_{\sigma_L}}$ calculated from equation (5) will not therefore be the true value of the pitching-moment curve slope but will be an effective value over the range of amplitudes up to the maximum amplitude measured. This is illustrated in figure 4 for a moment coefficient curve given by

$$C_m = -K\sigma^2 \tag{6}$$

[redacted]

As given in reference 4, a missile whose pitching motion is governed by this relation would yield the linear C_m curve shown on the figure if flown with a maximum angle of attack of 10°. It can be seen from this example that C_m, calculated from $C_{m_{\sigma_L}}$, does crudely approximate the static stability up to the maximum pitching amplitude displayed.

The problem of solving the complete equation of motion for the pitching and rolling missile with nonlinear restoring moment is very difficult, but in recent years solutions under certain restrictions have been developed (see e.g., refs. 4, 5, 7, and 8). The methods of references 4 and 5 are used in this report.

Kirk, in reference 4, presents a method of transforming linear theory results into the nonlinear expression for the pitching moment. The theoretical restrictions for the method to be valid are that the pitching motion be planar (trace in the α, β plane is linear and passes through the origin). However, it has been experimentally determined that this restriction is not rigid, and the method can be used successfully as long as the ratio $\sigma_{min}/\sigma_{max} \leq 1/3$. Sketch (a) illustrates the restriction imposed on the pitching motion for this method to be applicable.

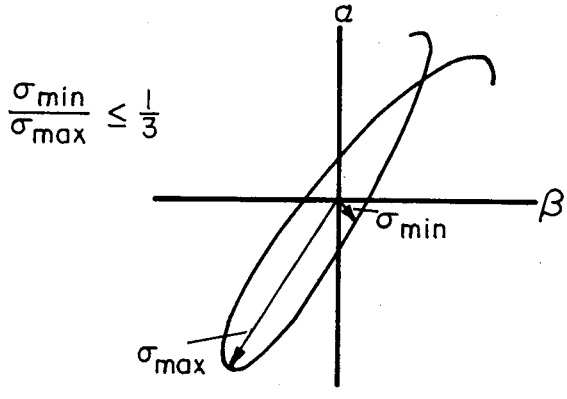

Sketch (a)

It is clear from presentations similar to that shown in figure 4 that the effective slope calculated by linear theory is equal in magnitude to the true slope at an angle of attack normally different from σ_{max}. Kirk has made this observation quantitative by assuming the pitching-moment coefficient in equation (1) to be described by nonlinear functions of amplitude, solving the resulting nonlinear differential equation thereby produced, and comparing these results with that given by the linear theory. In this manner he has been able to establish a relationship between σ_{max} and a fictitious σ_{eff} so that $C_{m_{\sigma_L}}$ at σ_{max} is equal to the true C_{m_σ} at σ_{eff}. The functional representations for C_m solved by Kirk are:

$$C_m = C\sigma^n \tag{7}$$

$$C_m = C(\sigma + a\sigma^3) \tag{8}$$

$$C_m = C(\sigma + a\sigma^2 + b\sigma^3) \tag{9}$$

[redacted]

$$C_m = C(\sigma + a\sigma^3 + b\sigma^5) \tag{10}$$

The relations used in this report are the linear-cubic (referred to as Kirk 1-3) and linear-cubic-quintic (referred to as Kirk 1-3-5) (eqs. (8) and (10)) in pitching amplitude to represent the variation of C_m. To apply this theory it is necessary to obtain from a series of flight tests the linear theory value $C_{m_{\sigma_L}}$ associated with σ_{max} for each test. Equation (5) is used for this purpose. As many discrete values of σ_{max} are required as there are unknown constants in the expression used for C_m (i.e., two for linear-cubic and three for linear-cubic-quintic). From the information contained in reference 4 these linear theory values can be transformed as follows:

A
4
5
6

$$\sigma_{max} \rightarrow \sigma_{eff}$$

$$C_{m_{\sigma_L}} = C_{m_\sigma}$$

This, then, gives the required number of points on the true C_{m_σ} curve, given by $dC_m/d\sigma$, to enable the unknown constant coefficients in the expression for C_m to be determined. Hence the problem is solved. The actual mechanics involved in the transformation $\sigma_{max} \rightarrow \sigma_{eff}$ are not extremely complicated for the 1-3 relation. However, for the 1-3-5 relationship it is almost a necessity to enlist the aid of an electronic computer.

The analysis developed by Rasmussen, in reference 5, for a moment curve described by $C_m = a\sigma + b\sigma^3$ begins with the general equations of motion for a symmetrical missile with zero trim. The solution of the nonlinear equation was found in closed form in terms of elliptic integrals under the above assumption for C_m. This method is valid for pitching motions radically different from planar as shown in sketch (b), so long as C_m can be represented by a linear plus a cubic term in σ.

The procedure used in the application of this method is described in reference 5. Briefly it relies on the very nearly linear behavior of the effective frequency of the pitching motion (defined by $\omega_e^2 = 4\pi^2 V^2/\lambda^2$) when plotted against $(\sigma_{max}^2 + \sigma_{min}^2)$. The intersection of the line described by this plot with the ω_e^2 axis is a measure of the coefficient of the linear term, and the slope of the line is a measure of the cubic term coefficient in the expression for C_m.

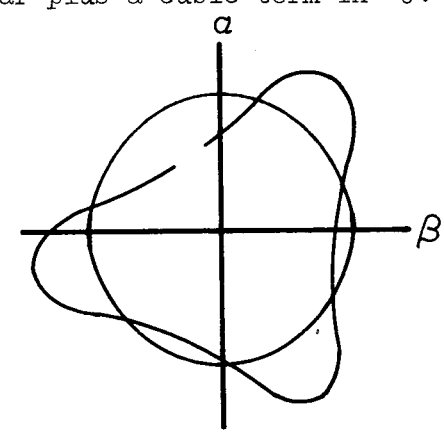

Sketch (b)

A critical comparison of the two methods just described is included in reference 4. For the case of purely planar motion with C_m actually defined by terms linear and cubic in σ the Kirk 1-3 and Rasmussen analyses agree. However, in the application of the Rasmussen theory, using the assumption of a linear relation between ω_e^2 and $(\sigma_{max}^2 + \sigma_{min}^2)$ can cause slight differences to occur.

RESULTS AND DISCUSSION

Experimental Stability Data

The data plotted in figure 5 as a function of maximum angle of attack are the values of $C_{m_{\sigma_L}}$ calculated by equation (5) for six runs with test model A. Table I lists the tunnel and model conditions for these six tests. The square symbols correspond to the more forward center-of-gravity location and therefore indicate greater stability. The presence of strong nonlinearity in the pitching moment is indicated by the increasing magnitude of $\left|C_{m_{\sigma_L}}\right|$ with increasing amplitude. A 4 5 6

Similar nonlinearity is evident in the data for test models B and C presented in tables II and III and figures 6 and 7.

Figure 8 is a presentation of the pitching moment for test model A as given by the Kirk 1-3 and 1-3-5 and the Rasmussen methods of data analysis. It can be seen that the pitching moment for the more stable configuration is equally well defined by any of these methods. For the less stable model the pitching moments determined by the Kirk 1-3 and Rasmussen methods are in close agreement but differ by a significant amount from that given by the Kirk 1-3-5 analysis. This difference is attributed to two major factors. First there is the mathematical influence of the quintic term in the expression for C_m, which necessarily affects the shape of the curve produced. Secondly and possibly more important for this model is the effect of data scatter. Because of the poor stability of this model, small relative changes in the three $C_{m_{\sigma_L}}$ values used can have a pronounced effect on the analysis and may cause the quintic term to change sign (i.e., change from a stabilizing to a destabilizing term, or vice versa). To eliminate this effect of data scatter it would be necessary to perform more tests and fair a curve through the $C_{m_{\sigma_L}}$ vs. σ_{max} data from which three more reliable values could be selected. If the data point for run 499 were lowered by only 4 percent (see fig. 5), the curve given by the Kirk 1-3-5 method would coincide with the Kirk 1-3 and Rasmussen results.

The normal-force coefficient and center-of-pressure location as a function of angle of attack can easily be determined from the two pitching-moment coefficient curves as the test models and testing conditions were nearly identical except for the center-of-gravity location. At any angle of attack the normal force and center-of-pressure location are independent of the center-of-gravity location. For a body tested with two center-of-gravity locations we can then write for a given angle of attack

$$\left.\begin{aligned} C_{m_1} &= C_N\left(\frac{X_{cg_1}}{l} - \frac{X_{cp}}{l}\right) \\ C_{m_2} &= C_N\left(\frac{X_{cg_2}}{l} - \frac{X_{cp}}{l}\right) \end{aligned}\right\} \qquad (11)$$

A456

Solving for C_N and $\frac{X_{cp}}{l}$ we get

$$C_N = \frac{C_{m_1} - C_{m_2}}{\frac{X_{cg_1}}{l} - \frac{X_{cg_2}}{l}} \qquad (12)$$

and

$$\frac{X_{cp}}{l} = \frac{C_{m_1}\frac{X_{cg_2}}{l} - C_{m_2}\frac{X_{cg_1}}{l}}{C_{m_1} - C_{m_2}} \qquad (13)$$

Applying equations (12) and (13) to the information in figure 8 we arrive at the results presented in figure 9. The normal force is seen to be nearly a linear function of the angle of attack up to $\sigma = 6^{\circ}$; therefore the slight nonlinearity of the pitching moment in this region must be due to the rearward movement of the center of pressure. Note that the less stable model displays a more nonlinear pitching moment in this region than the more stable configuration. This is due to the shorter moment arm from the center of pressure to the center of gravity for this model, which causes it to be more sensitive to changes in the center-of-pressure location. Above $\sigma = 6^{\circ}$ the normal force increases in a nonlinear manner, causing the pitching moment to greatly increase its nonlinear behavior.

The pitching moment for test model B is shown in figure 10. The Kirk 1-3-5 method could not be employed in this case, as the third test displayed an almost circular α, β motion (symbol with a tic in fig. 6). The Rasmussen and Kirk 1-3 methods agree very well and indicate that this model possesses very good static stability even though the center of gravity is located at $0.490l$ from the nose. Plotted also on this figure is the pitching moment for model A with $X_{cg} = 0.490l$. It is

clear that the larger flare and blunter nose have a pronounced effect on the static stability of this model. Normal force and center of pressure could not be determined in this case, as only one center-of-gravity location was tested.

The data scatter in the low amplitude region for test model C made the analysis of this body less exact than that of test models A and B. This scatter is attributed to small differences in center-of-gravity location, as noted in table III, and to the inherent difficulty in defining the wave length of pitching motion when σ_{max} is small and the stability is poor. Because of the unknown influence of these factors on the data points, the three low amplitude tests were averaged to obtain a single point at $\sigma_{max} = 7.1^{\circ}$ and $C_{m_{\sigma_L}} = -0.105$. The pitching moments given by the Rasmussen and Kirk methods are shown in figure 11. The Rasmussen analysis has been applied separately to the low- and the high-amplitude regions. For this method of presentation to be meaningful it is necessary that, for the angle of attack interval included, C_m be closely approximated by a linear-cubic expression. This assumption is probably very good for the low-amplitude region shown. For high-amplitude regions, the greater effect of higher ordered terms in the actual C_m relation limits the linear-cubic approximation to small angle of attack intervals. The high-amplitude region shown (19° to 32°) in this figure is very likely much too large and therefore is not considered quantitatively valid but does indicate the necessity of using higher order terms to describe the pitching moment over a wide range of amplitudes. The Kirk 1-3 method is applied only to the low-amplitude region and, as previously established for models A and B, agrees substantially with the Rasmussan analysis.

The Kirk 1-3-5 analysis indicates a rapid decrease in stability above 28°, becoming unstable at 36°. It is expected that at very large angles of attack, the pitching moment would tend to approach a limit or possibly would decrease somewhat, but a rapid decrease and particularly the complete loss of stability for this model is doubtful. The true pitching-moment representation over a large range of pitching amplitudes would be a very complicated function because of boundary-layer separation and shock wave and body interaction. The simplicity assumed by limiting the polynomial expansion of C_m to a linear-cubic-quintic relation thus restricts the method and should be used with caution whenever the range of values of σ_{max} becomes large; extrapolation to higher angles should particularly be avoided. To apply the Kirk 1-3-5 analysis properly to the small angle region, then, other tests with σ_{max} falling in the range 12° to 14° would be desired. For this reason it is believed that the results from the Rasmussen and Kirk 1-3 analyses are more reliable for this test model, in the pitching amplitude range $0 < \sigma < 10^{\circ}$.

All three of these methods indicate that this model is slightly unstable at $\sigma = 0$, becoming stable at about 3°. This low initial stability is caused, in part at least, by the small half angle of the flare (9.1°). The main effect of a modest increase in flare angle would be to cause the center of pressure of the flare to move rearward, thereby increasing the stability. The more rapid increase in the pitching moment of this model with angle of attack (as compared with models A and B) is primarily due to the large plan-form area of the flare, which has a pronounced effect on the flare normal force when the model is rotated to an angle of attack. Also not to be overlooked is the very sensitive nature of models with poor stability to small changes in the location of the center of pressure, as noted in the discussion of model A.

A
4
5
6

Newtonian impact theory is used as a comparison with the experimental pitching moments determined. The values shown in figures 12(a), (b), and (c) are extensions of the initial slopes given in reference 9. Figure 12 shows that at these Mach numbers impact theory overpredicts the static stability considerably and in the case of test model C fails to give any indication of the instability at very low amplitude. Reference 3 presents a discussion of some of the reasons that impact theory should be expected to overpredict the static stability of missiles of this general configuration at hypersonic velocities.

Reference 3 also presents a theoretical method of predicting the static stability contributed by the flare and a semiempirical method for the forebody, calculated by perturbation of the zero angle-of-attack pressure distribution. The pitching-moment estimations by this method are also compared with the experimental data in figure 12.

The value of this method is clearly seen to be the ability to closely predict the initial static stability. This is particularly true for test models B and C. The limitation of the method at higher angles of attack is, as discussed in reference 3, very likely due to the treatment of the forebody contribution to over-all stability. This belief is supported by the normal force and center-of-pressure comparisons with model A made in figure 9. This figure indicates that the initial normal-force curve slope is very accurately predicted and the normal-force prediction is good up to $\sigma = 5^{\circ}$. The greatest error in the stability prediction is therefore caused by a $0.05l$ error in center-of-pressure location. The center of pressure of the flare can be located with a reasonable degree of certainty and consequently the major error in the center-of-pressure location must be attributed to the forebody. This point is further illustrated by figure 13, which shows that, theoretically, the normal force contributed by the forebody is two to three times that contributed by the flare, indicating the relatively greater influence of the forebody in the location of the center of pressure.

Drag

Figure 14 presents the drag coefficients of the subject models plotted against the root mean square angle of attack. Note the similarity between the drag coefficients of test models A and C in the low-angle region. This correlates with the fact that they have nearly identical nose shapes and flare base diameters. The data shown in this plot are also tabulated in tables I, II, and III.

CONCLUDING REMARKS

Each of the test models reported herein displays poor initial static stability and strong nonlinearity of the pitching moment with amplitude consistent with the data given in references 2 and 3. The experimental results have been compared with the Newtonian impact theory and the theory of reference 3. The Newtonian theory has been established beyond a doubt in this report and in others to be an unreliable method of predicting the static stability of this class of missiles. The theory described in reference 3 gives a usefully accurate estimate of the initial (small angle) stability of blunt-nosed flare stabilized bodies, at least for the bodies and speeds investigated in the present study. It should, however, as noted by its originators, be improved in its treatment of the center-of-pressure location of the forebody, because it fails to indicate the strong favorable nonlinearity that appears at angles of attack of the order of a few degrees.

The theoretical methods developed by Rasmussen and Kirk for reducing stability coefficients from free-flight test data have been applied to the three test models and have been found easy to apply and to agree very well where comparison was possible.

Ames Research Center
National Aeronautics and Space Administration
Moffett Field, Calif., Dec. 12, 1960

REFERENCES

1. Reese, David E., Jr., and Wehrend, William R., Jr.: An Investigation of the Static and Dynamic Aerodynamic Characteristics of a Series of Blunt-Nosed Cylinder-Flare Models at Mach Numbers From 0.65 to 2.20. NASA TM X-110, 1960.

2. Carros, Robert J.: Free-Flight Investigation of Static Stability and Drag of Models of the Second and Third Stages of the Hemisphere-Nosed X-17 at Mach Numbers From 4 to 10. NASA TM X-158, 1960.

3. Seiff, Alvin, and Whiting, Ellis: The Effect of the Bow Shock Wave on the Stability of Blunt-Nosed Slender Bodies. NASA TM X-377, 1960.

4. Kirk, Donn B.: A Method for Obtaining the Nonlinear Aerodynamic Stability Characteristics of Bodies of Revolution From Free-Flight Tests. NASA TN D-780, 1961.

5. Rasmussen, Maurice L.: Determination of Nonlinear Pitching-Moment Characteristics of Axially Symmetric Models From Free-Flight Data. NASA TN D-144, 1960.

6. Bioletti, Carlton, and Cunningham, Bernard E.: A High-Velocity Gun Employing a Shock-Compressed Light Gas. NASA TN D-307, 1960.

7. Murphy, Charles H.: The Measurement of Nonlinear Forces and Moments by Means of Free-Flight Tests. Ballistic Research Lab. Rep. 974, Feb. 1956.

8. Murphy, Charles H.: The Prediction of Nonlinear Pitching and Yawing Motion of Symmetric Missiles. Jour. Aero. Sci., vol. 24, no. 7, July 1957, pp. 473-479.

9. Fisher, Lewis R.: Equations and Charts for Determining the Hypersonic Stability Derivatives of Combinations of Cone Frustums Computed by Newtonian Impact Theory. NASA TN D-149, 1959.

A
4
5
6

TABLE I.- TEST CONDITIONS AND RESULTS FOR MODEL A

Run No.	M_∞	$R \times 10^{-6}$ $\frac{\rho V l}{\mu}$	$\rho \times 10^3$ $\frac{slug}{ft^3}$	$I \times 10^6$ $slug\text{-}ft^2$	$\frac{X_{cg}}{l}$	l, in.	σ_{max}, deg	σ_{min}, deg	$\sqrt{\overline{\sigma^2}}$, deg	λ, ft	$-C_{m_{\sigma_L}}$, $\frac{8\pi^2}{\lambda^2}\frac{I}{\rho A l}$	C_D
448	16.0	5.49	0.9015	0.234	0.3971	1.0274	5.4	1.3	3.9	50.8	0.260	0.6112
450	14.4	4.96	.9061	.235	.3993	1.0275	18.4	1.0	13.0	29.5	.754	.8518
546	14.9	8.44	1.515	.235	.3996	1.0279	13.9	1.3	9.9	27.7	.516	.6982
499	14.2	6.24	1.492	.0576	.4584	.7956	9.3	2.6	6.8	33.8	.184	.6456
513	16.0	7.46	1.592	.0581	.4577	.7965	13.2	.8	9.4	27.5	.264	.6751
550	17.3	8.06	1.590	.0580	.4560	.7970	7.5	.3	5.1	37.2	.143	.5952

TABLE II.- TEST CONDITIONS AND RESULTS FOR MODEL B

446	16.2	5.97	.8825	.319	.4850	1.1277	14.5	.5	10.3	42.8	.388	1.0380
451	13.6	5.34	.9252	.312	.4936	1.1265	8.7	5.5	7.3	47.6	.294	.9660
454	16.1	5.99	.8917	.319	.4898	1.1286	10.0	2.2	7.2	51.8	.260	.9482

TABLE III.- TEST CONDITIONS AND RESULTS FOR MODEL C

503	13.2	5.97	1.528	.0441	.4035	.8066	19.0	3.6	13.7	18.3	.820	.9820
505	13.4	5.94	1.512	.0437	.4086	.8062	32.0	8.6	23.4	16.1	1.065	1.8020
554	16.0	7.08	1.507	.0436	.4080	.8062	8.1	1.8	5.9	53.8	.096	.6230
595	16.4	7.15	1.482	.0502	.4011	.8068	6.5	.7	4.6	54.8	.108	.5820
608	16.3	7.34	1.532	.0503	.4004	.8059	6.6	.2	4.7	52.0	.115	

[redacted]

[redacted]

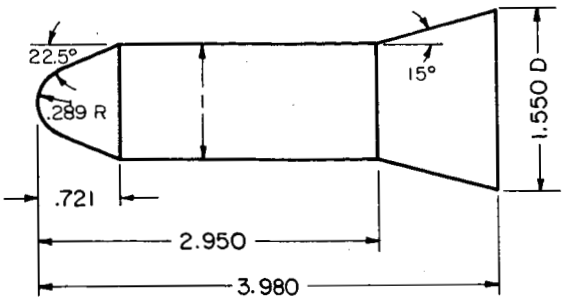

(a)
Model A

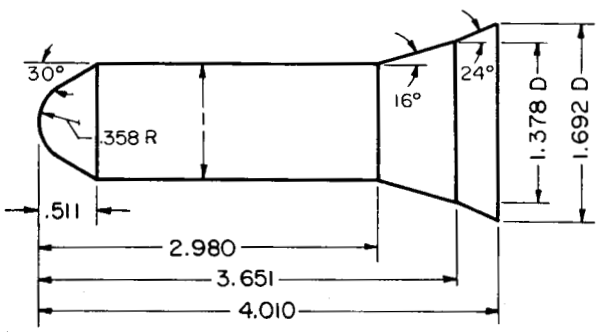

(b)
Model B

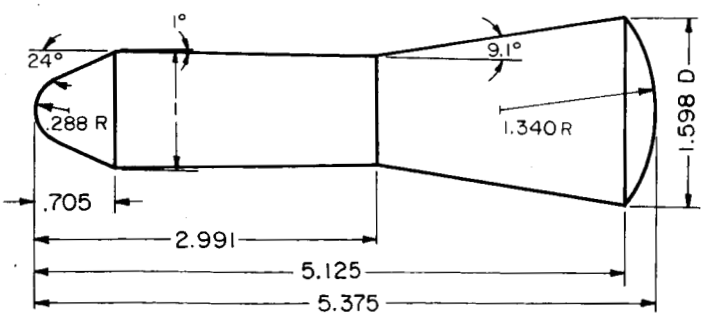

(c)
Model C

Figure 1.- Models tested (all dimensions in terms of diameter at nose-body juncture).

[redacted]

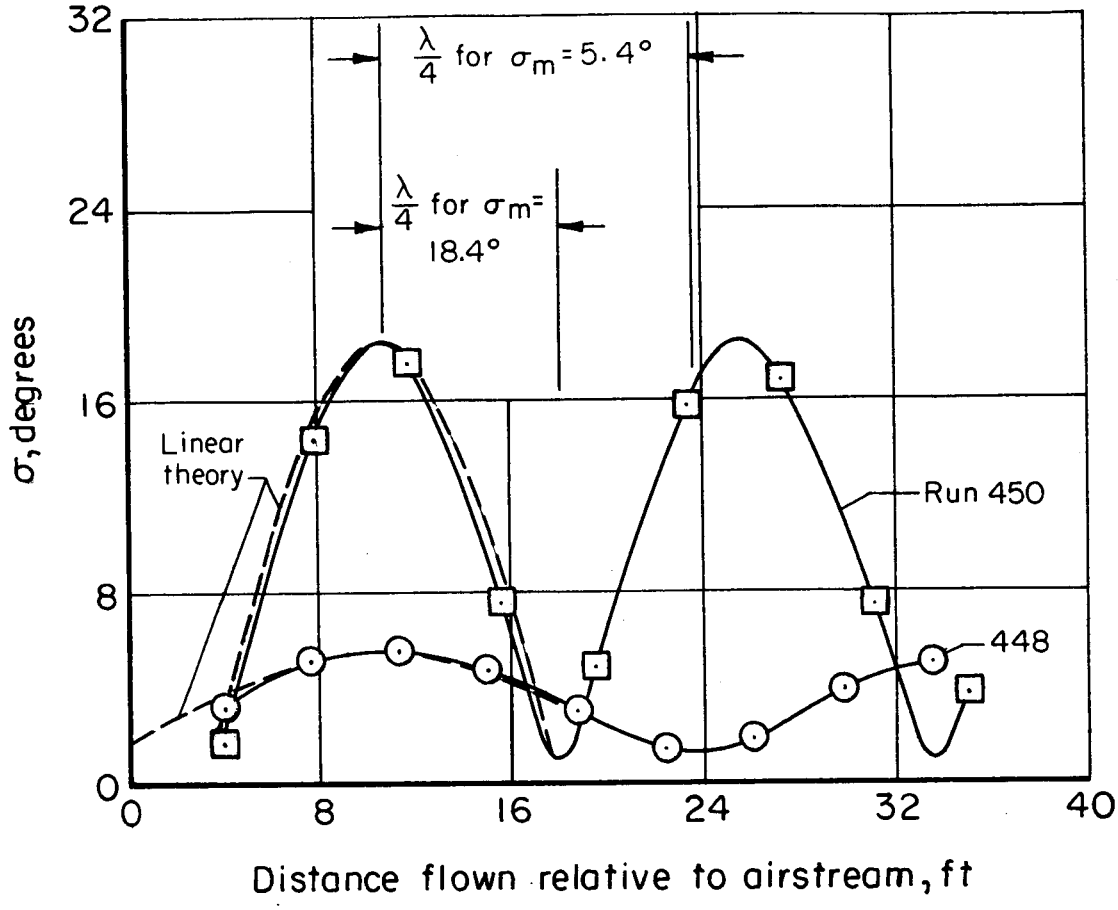

Figure 2.- Resultant angle-of-attack history for two test runs and comparison with linear theory.

A456

[redacted]

A
4
5
6

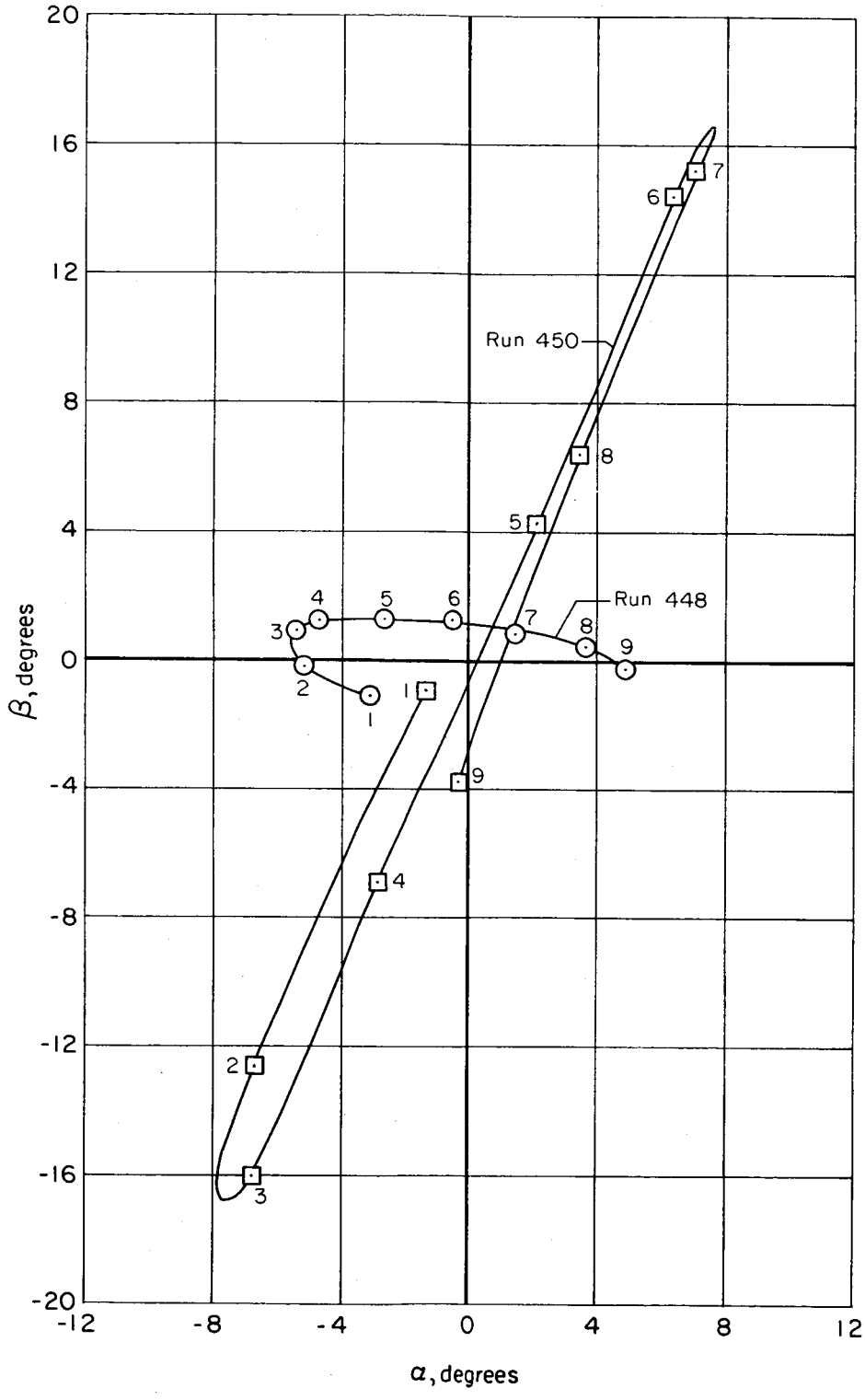

Figure 3.- Motion in α, β plane for two test runs.

[redacted]

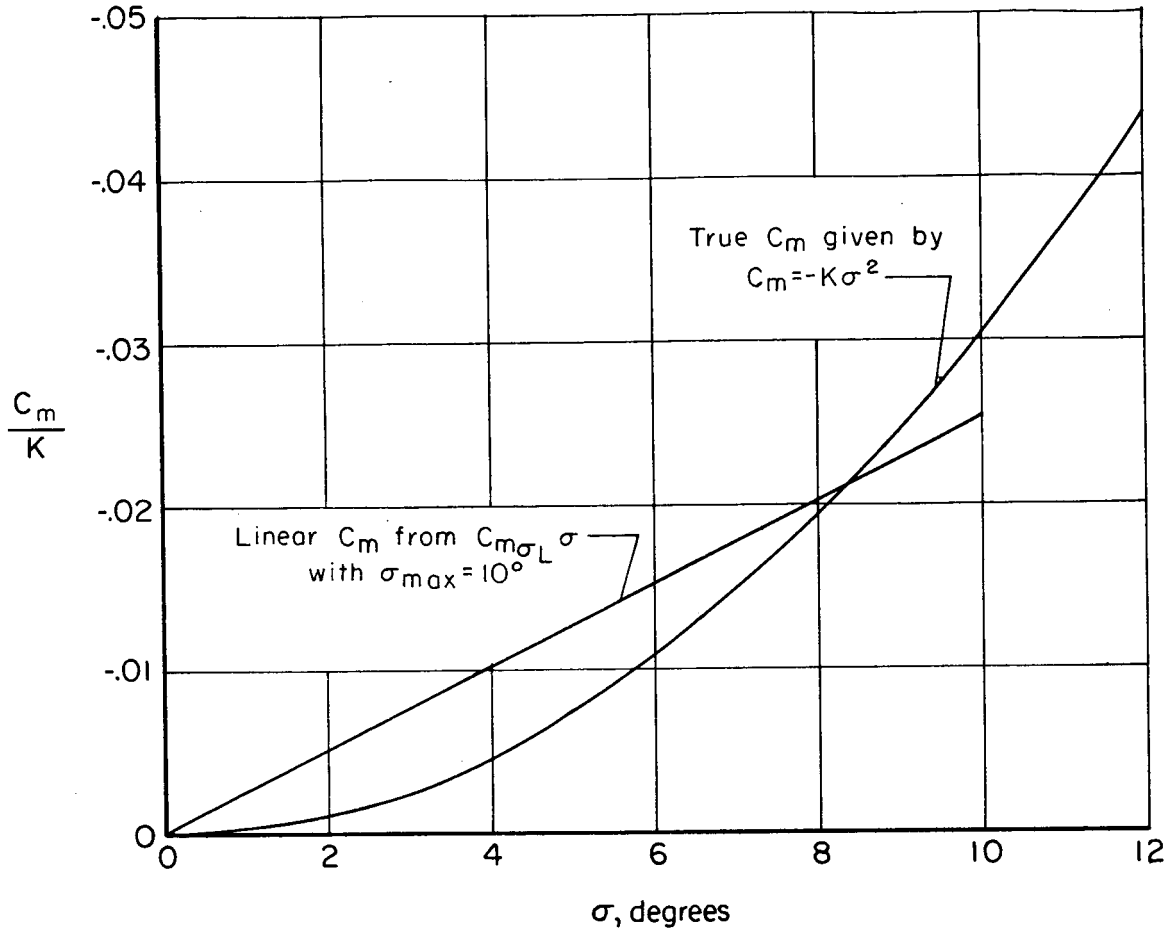

Figure 4.- Comparison of a nonlinear pitching-moment curve with linear solution corresponding to $\sigma_{max} = 10^{\circ}$.

[redacted]

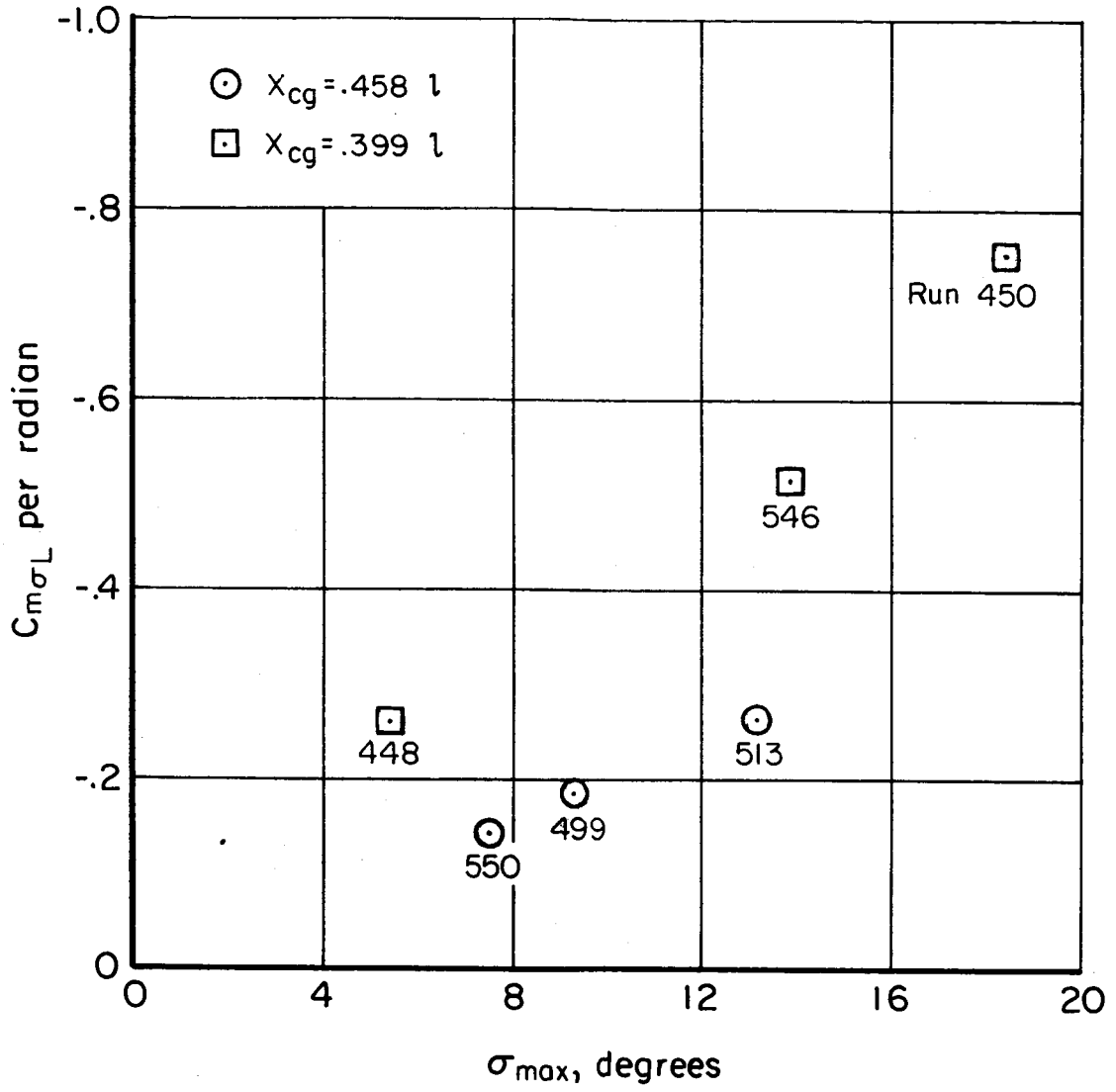

Figure 5.- Linear pitching-moment curve slope as a function of maximum resultant angle of attack for model A.

A
4
5
5

[redacted]

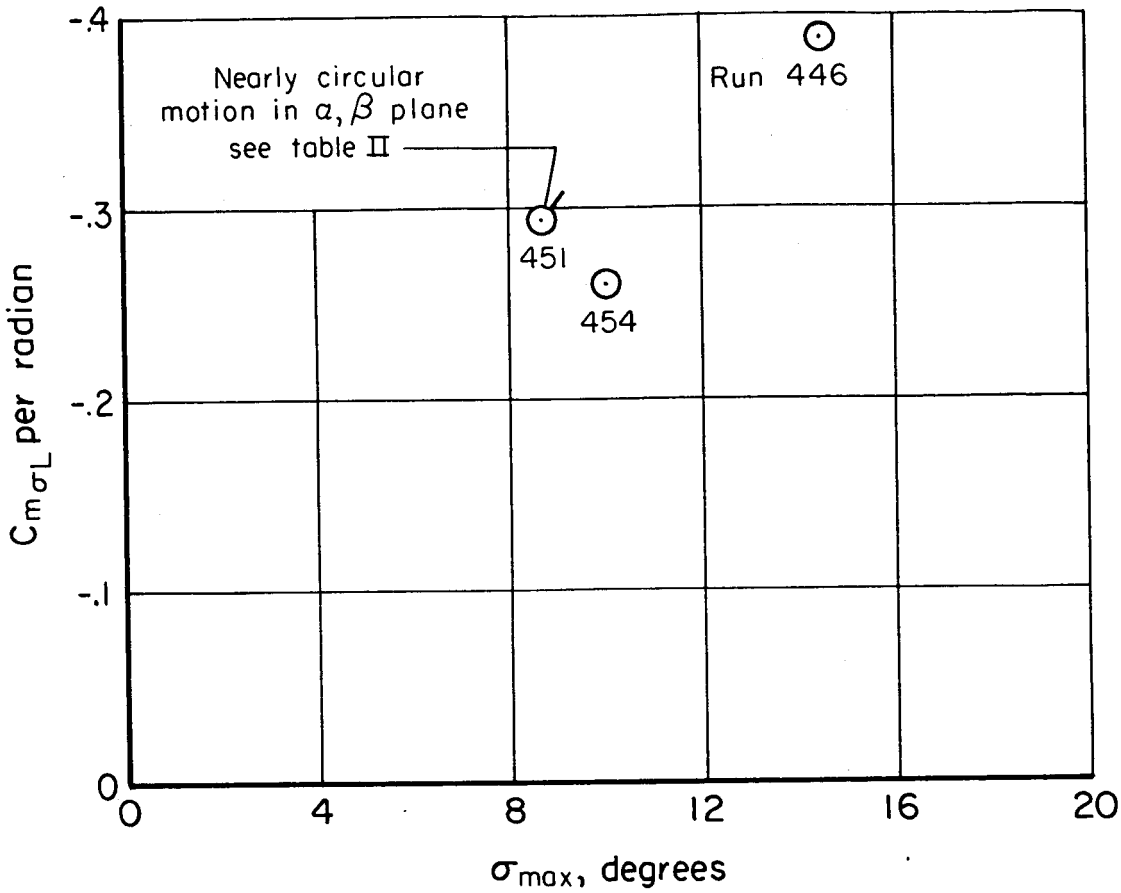

Figure 6.- Linear pitching-moment curve slope as a function of maximum resultant angle of attack for model B.

A
4
5
6

[redacted]

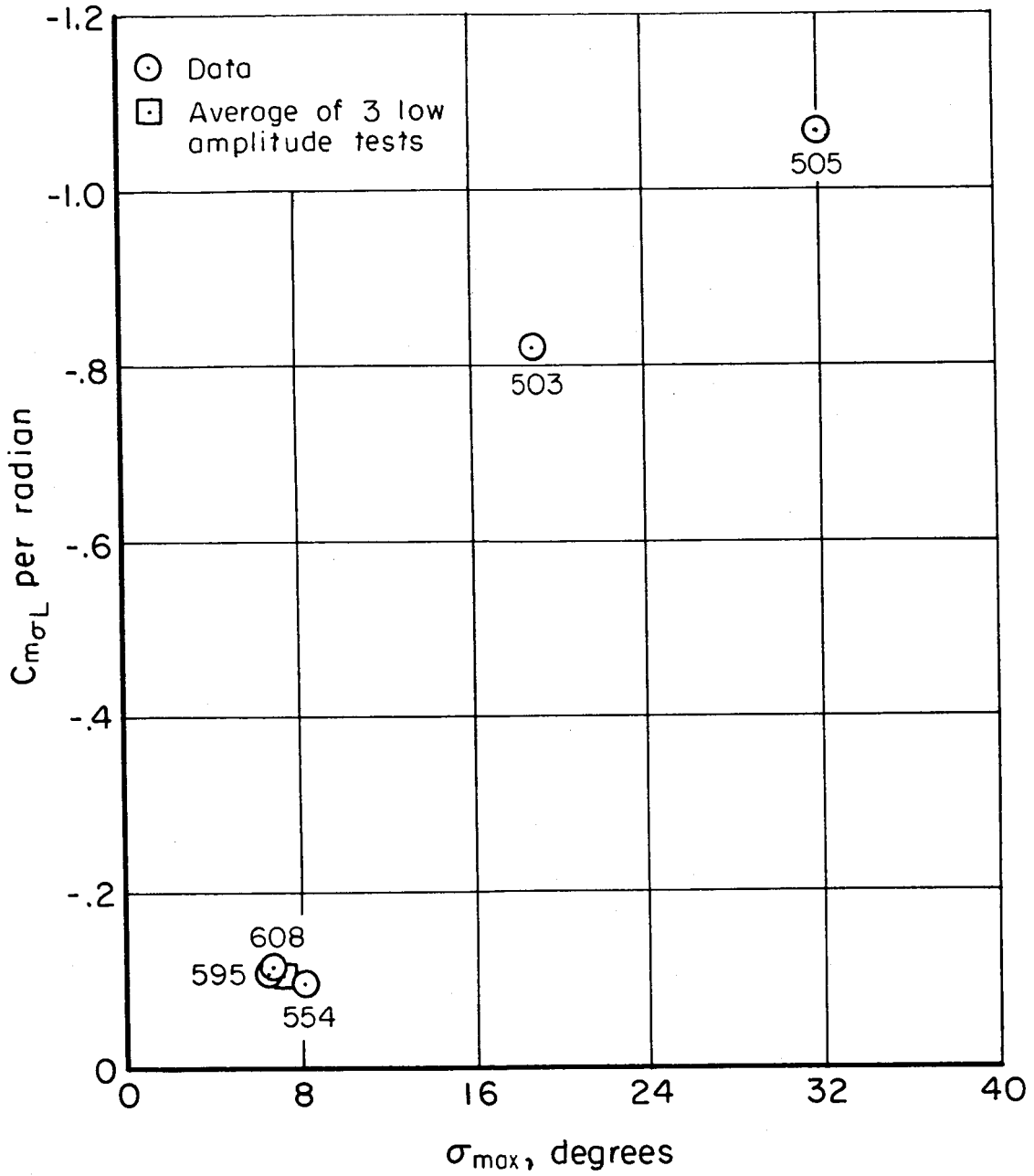

Figure 7.- Linear pitching-moment curve slope as a function of maximum resultant angle of attack for model C.

A
4
5
6

[redacted]

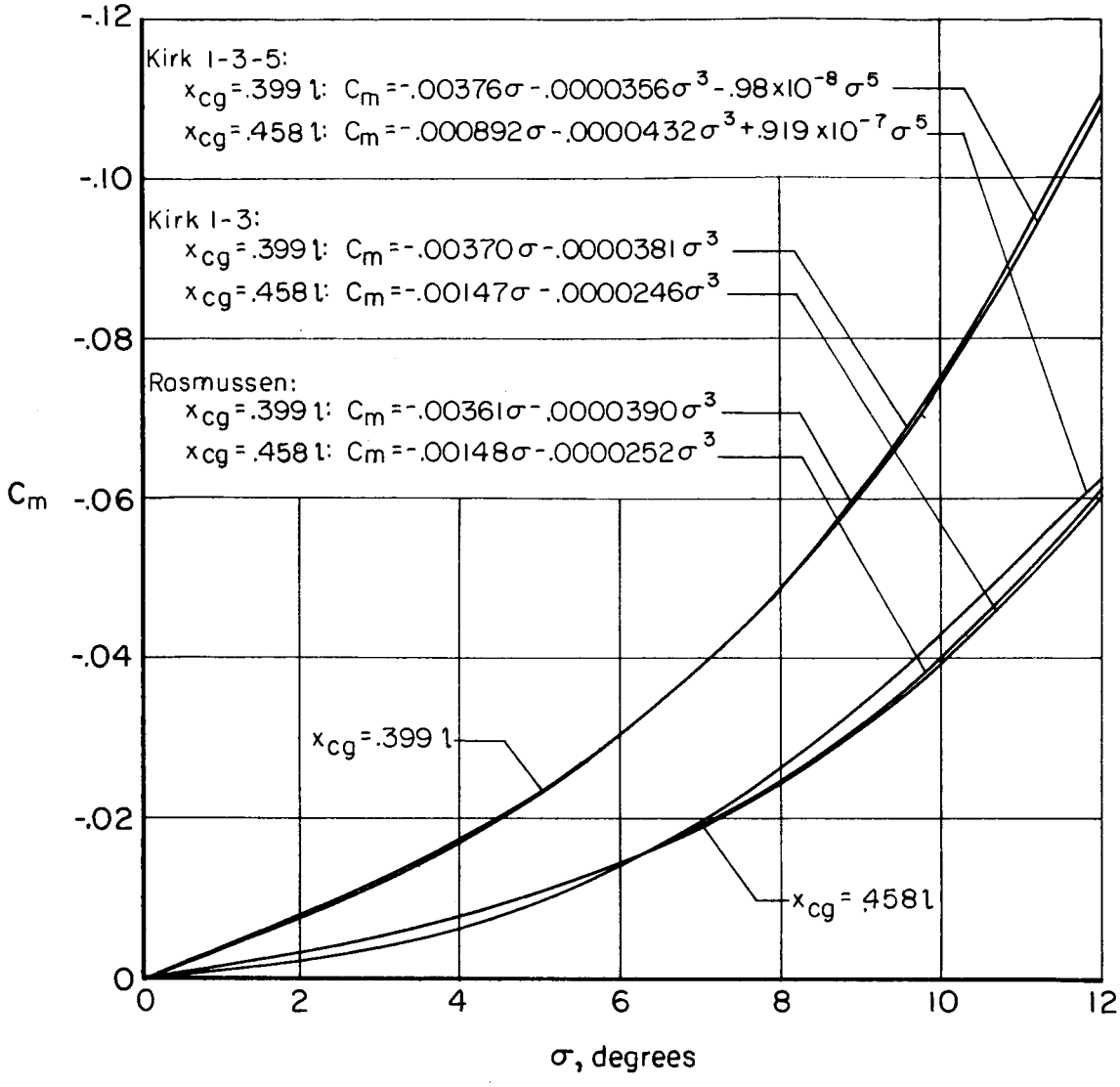

Figure 8.- Pitching-moment coefficient as a function of resultant angle of attack for model A as given by three methods of data analysis.

[redacted]

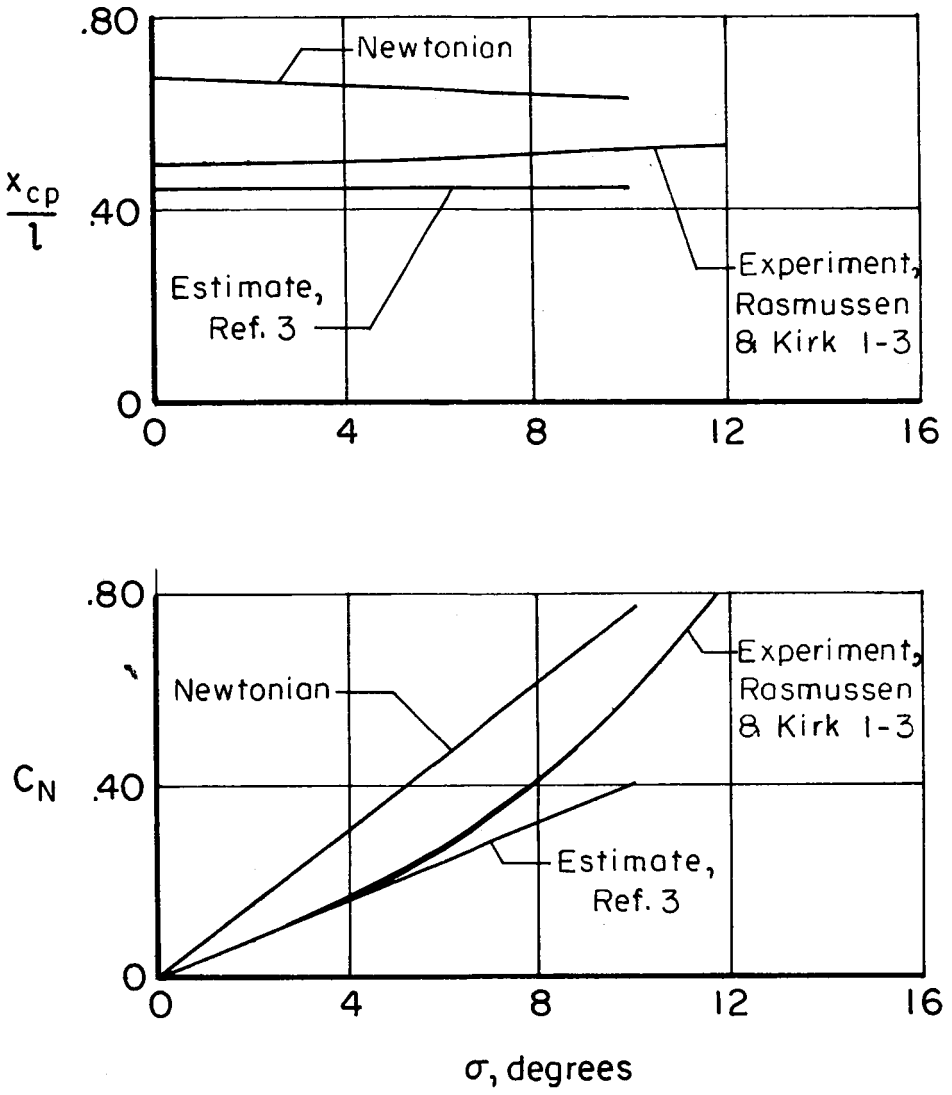

Figure 9.- Center-of-pressure location and normal-force coefficient as a function of the resultant angle of attack for model A.

[redacted]

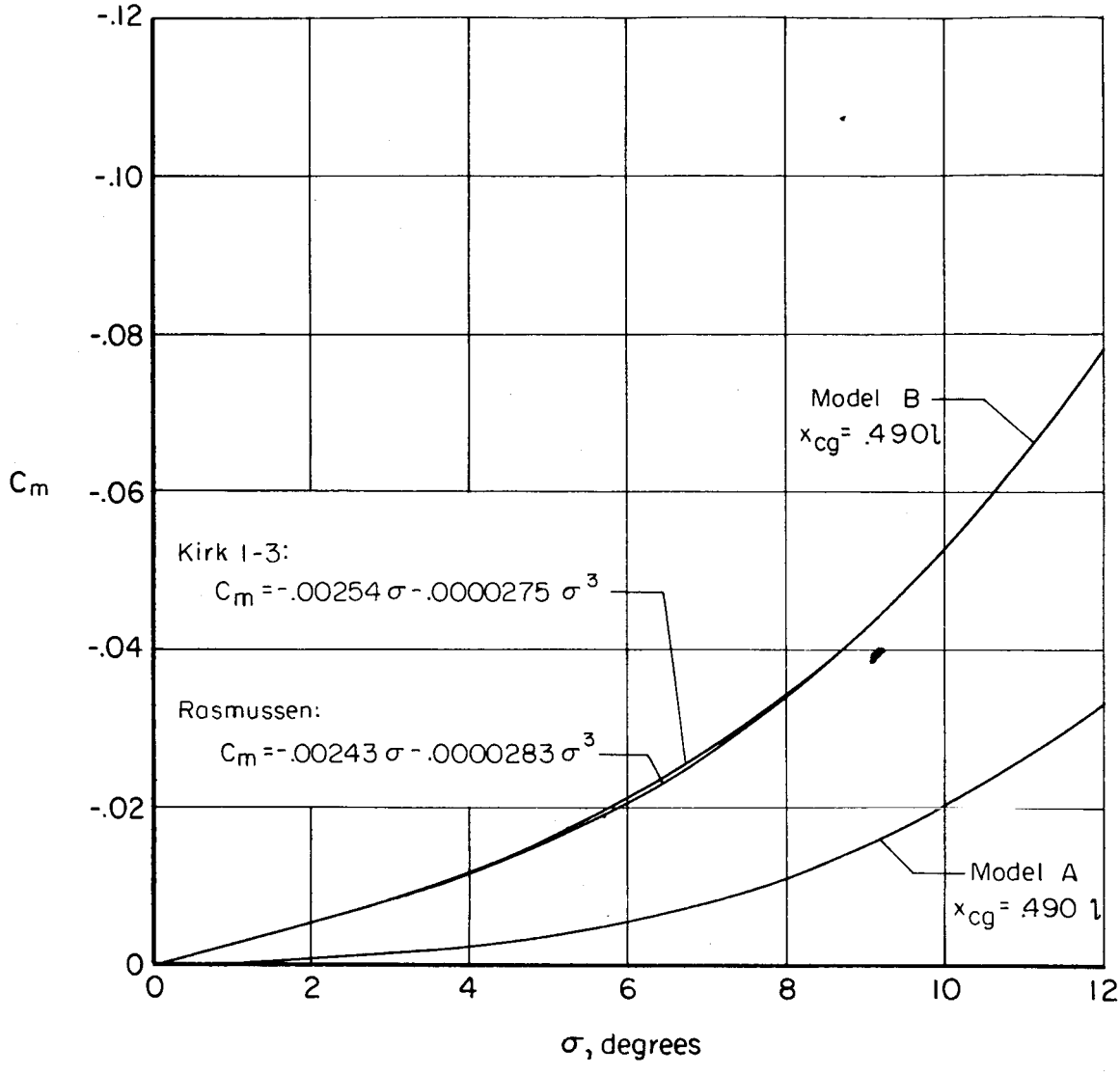

Figure 10.- Pitching-moment coefficient as a function of resultant angle of attack for model B as given by two methods of data analysis.

[redacted]

[redacted]

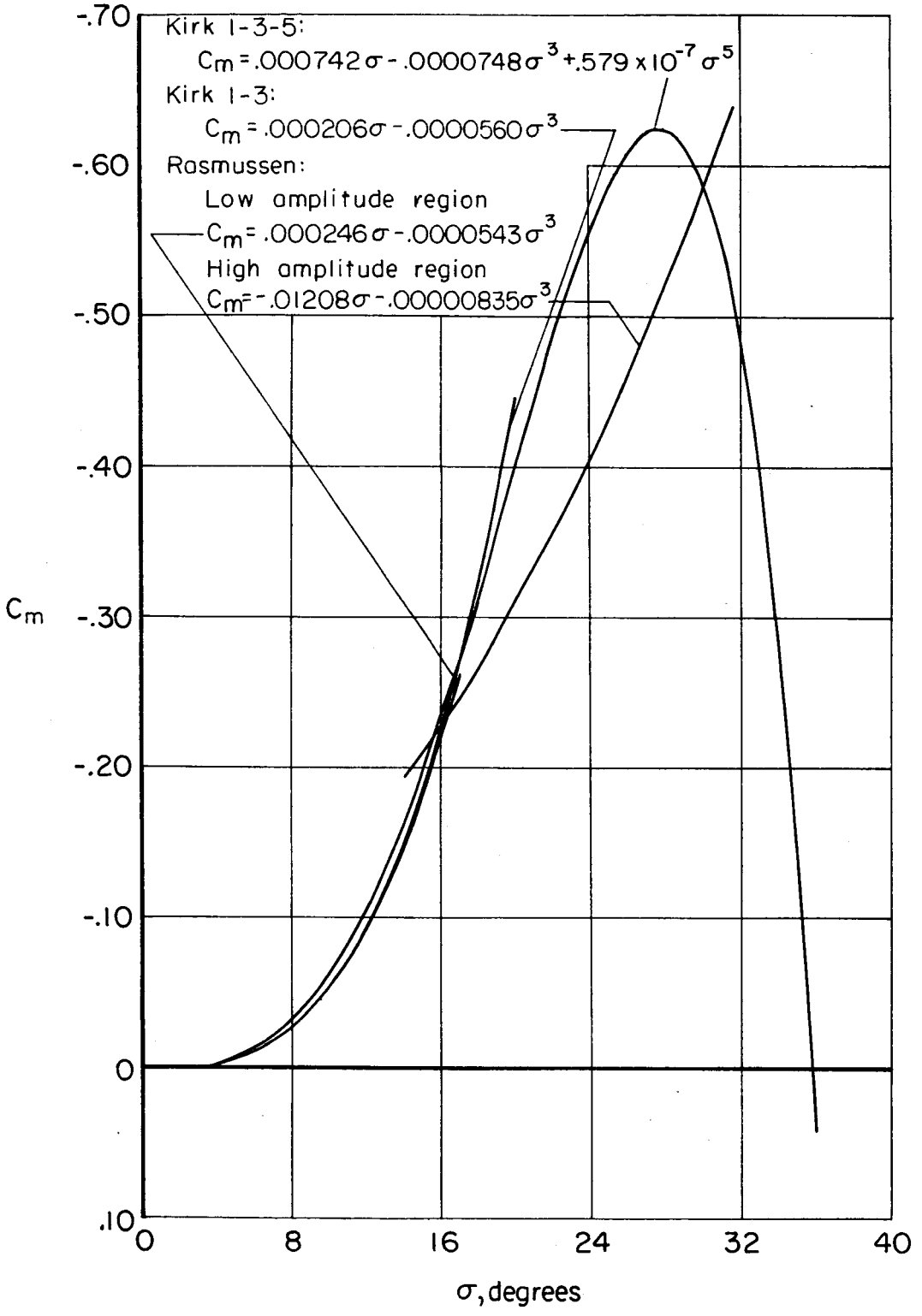

Figure 11.- Pitching-moment coefficient as a function of resultant angle of attack for model C as given by three methods of data analysis.

[redacted]

[redacted]

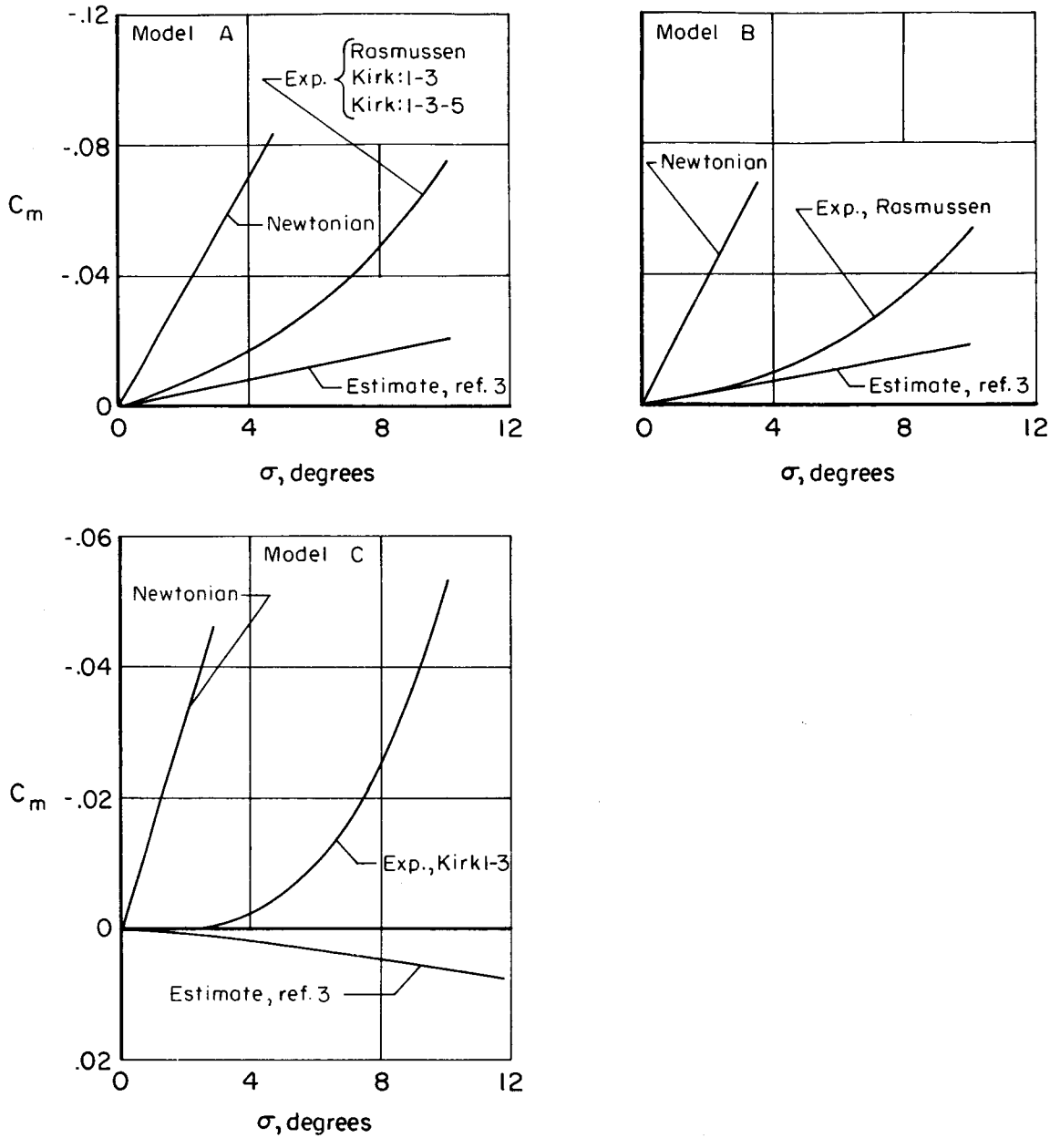

Figure 12.- Comparison of experimentally determined moment curves with two estimation procedures.

[redacted]

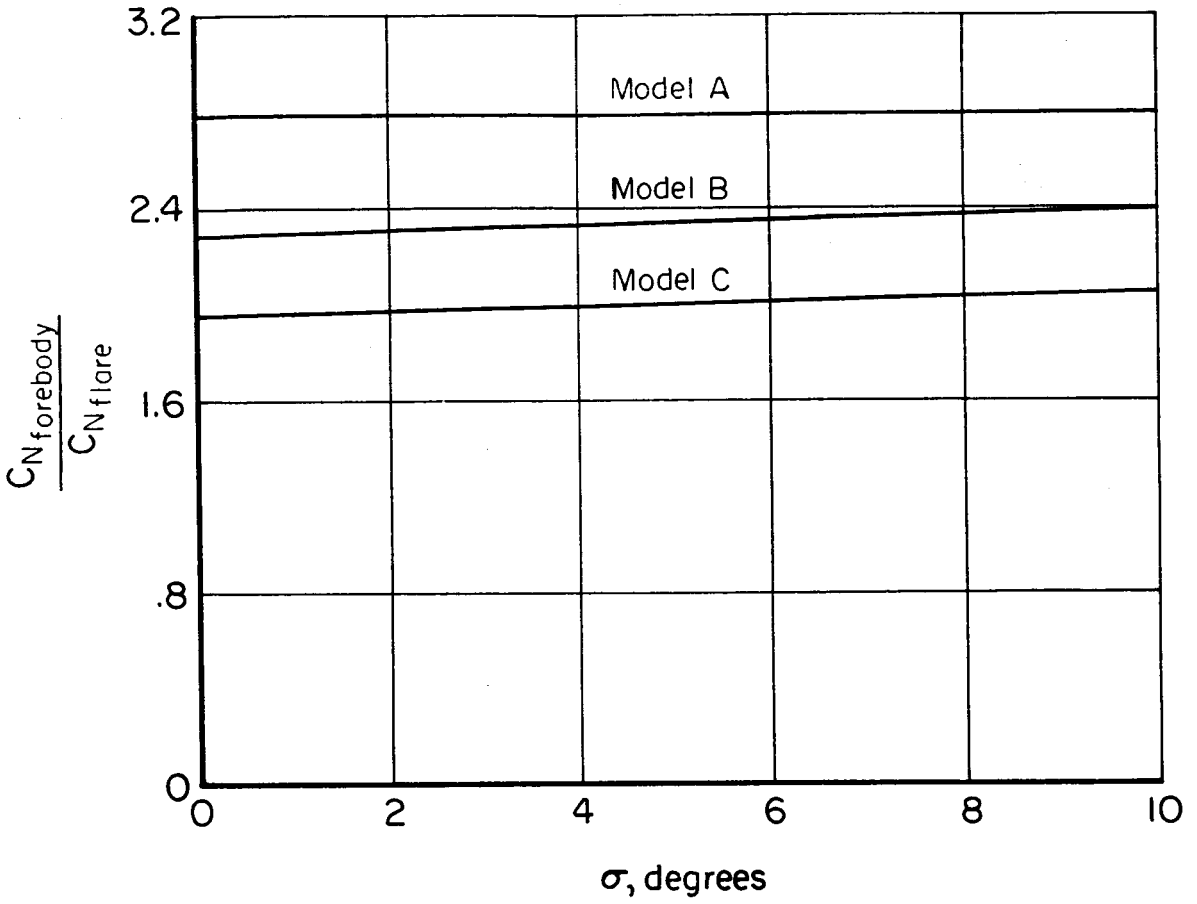

A
4
5
6

Figure 13.- Ratio of the normal-force contribution of the forebody to the normal force acting on the flare as given by the estimation procedure of reference 3.

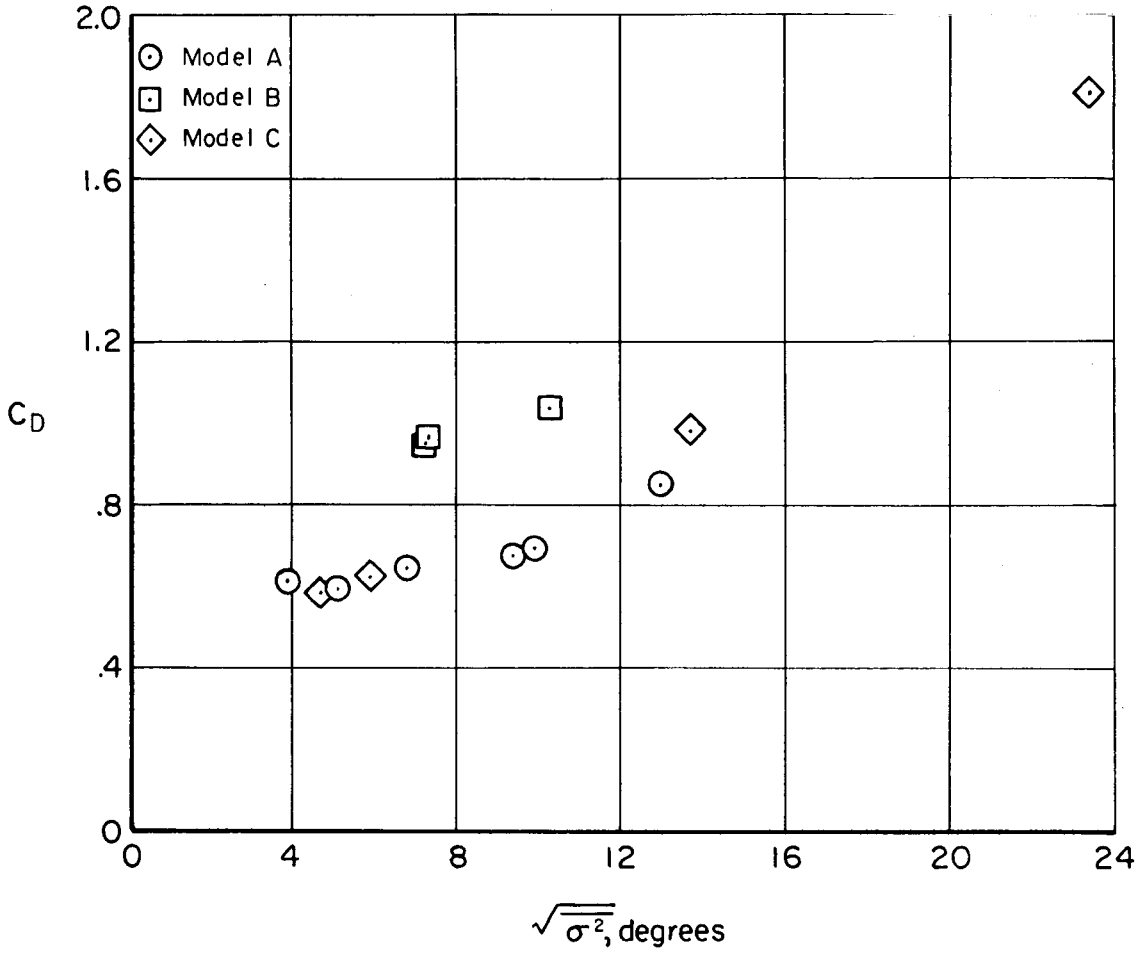

Figure 14.- Drag coefficient as a function of root mean square angle of attack for models A, B, and C.

A
4
5
6

NASA - Langley Field, Va. A-456